

¹ **On using Computational Aeroacoustics for**
² **Long-Range Propagation of Infrasonds in Realistic**
³ **Atmospheres**

C. Millet,¹ J.-C. Robinet,² and C. Roblin^{1,2}

C. Millet, CEA, FRANCE. (christophe.millet@cea.fr)

¹Laboratoire de Géophysique, CEA,
Bruyère-le-Châtel, FRANCE.

²Laboratoire de Simulation Numérique en
Mécanique des Fluides, ENSAM, Paris,
FRANCE.

4 In this study, a perturbative formulation of non linear euler equations is
5 used to compute the infrasound propagation in real atmospheres. Based on
6 a Dispersion-Relation-Preserving numerical scheme, the discretization pro-
7 vides very good properties for both sound generation and long range infra-
8 sound propagation over a variety of spatial atmospheric scales. The back-
9 ground flow is obtained by matching the comprehensive empirical global model
10 of horizontal winds HWM-93 with radio and rocket soundings of the lower
11 atmosphere. Comparison of calculations and experimental data from the ex-
12 plosive “Misty Picture” test (on May 14, 1987) shows that asymptotic tech-
13 niques based on high frequency approximations **cannot explain** some im-
14 portant features of the measurements. The small scales of high resolution me-
15 teorological data provide important changes in the detection predictions and
16 the emergence of large-scale coherent structures of atmospheric turbulence.

1. Introduction

17 Due to the development of the method of infrasonic monitoring of nuclear explosions,
18 many attempts have been made to model the long-range propagation of low-frequency
19 acoustic (infrasonic) waves throughout the atmosphere. There is now a substantial body
20 of theoretical and experimental evidence that the infrasonic signals, that are recorded at
21 long distances from surface explosions, consist of several main components, namely, Lamb
22 waves, tropospheric, stratospheric, mesospheric and thermospheric arrivals. These waves
23 propagate along cyclic ray paths characterized by different heights of turning toward the
24 ground surface (see Kulichkov [1992] for a review).

25 Unlike many fluid dynamics problems in which computational methods have played an
26 important role in their solution, most infrasound propagation problems are still solved
27 principally by asymptotic techniques. Presently, a consensus seems to have emerged that
28 these techniques most probably cannot explain some important arrivals in the microbaro-
29 graph measurements (**see, for instance, Ponomarev *et al.* [2006], Kulichkov *et al.***
30 **[2004, b, 2002]**). In the present work, a new generation of numerical methods is used in
31 order to simulate both the non linear propagation of infrasounds throughout a fine lay-
32 ered atmosphere and the large-scale coherent turbulence that develop in the atmosphere.
33 The method is based on a time marching Dispersion-Relation-Preserving (DRP) scheme
34 (see Bogey & Bailly [2004] for a recent review), which is now used in length in compu-
35 tational aeroacoustics. Since the attention is focused on the impact of small atmospheric
36 structures, the non linear Euler equations are considered with no assumption. The Misty

37 Picture experiment is considered as a benchmark problem and the results are compared
38 to both experimental data and results of asymptotic techniques.

2. Basic asymptotic techniques

39 Three basic approaches may be distinguished to model the long-range propagation of
40 acoustic waves. They are the geometric acoustics approximation or ray tracing, the normal
41 mode method and the parabolic equation method. The ray tracing is most commonly used
42 by the geophysical community as it permits to qualitatively explain the basic properties
43 of infrasonic signals observed during experiments. However, this approximate method
44 is restricted to high frequency waves, and it fails to predict some important mean flow
45 refraction effects in meteorological flows such as mountain wakes or jet streams. Such
46 flows are known to support coherent structures of turbulence.

47 For specific sound speed vertical profiles, exact normal mode solutions of the acoustic
48 wave can be obtained, as those of Raspet *et al.* [1991, 1992] or Attenborough *et al.* [1995],
49 for a downward refracting atmosphere. Approximate solutions may be obtained when the
50 sound and wind speed vary slowly with height, but in all other cases the problem has to
51 be solved numerically. More recently, Kulichkov *et al.* [2004, b] used a pseudodifferential
52 parabolic equation to interpret fast infrasonic arrivals that cannot be obtained with the
53 ray tracing.

54 Although these approximate methods are not equivalent, they all have a limited range of
55 validity and can fail at low frequencies. Indeed, for explosions equivalent or less than 1 kt
56 of TNT, infrasonic wavelengths vary from hundred of meters to units of kilometers, which
57 is comparable with both temperature and wind scales of the conventional meteorological

58 data. Thus, it is imperative for an accurate prediction to solve the fully non linear Euler
59 equations. These equations, in one form or another, have become the *de facto* standard
60 for noise propagation prediction schemes in aeroacoustics problems.

3. The Dispersion-Relation-Preserving approach

61 For time dependent problems, especially acoustics problems, it is known that a consis-
62 tent, stable and convergent high order scheme does not guarantee a good quality numeri-
63 cal wave solution. According to the wave propagation theory (e.g. Whitham [1974]), the
64 propagation characteristics of the waves governed by Euler equations are encoded in the
65 dispersion relation in the frequency and wave number space. Following the early studies
66 of Tam & Webb [1993] and Tam & Dong [1996], the time marching scheme used in this
67 study is obtained by optimizing the finite difference approximations of the space and time
68 derivatives in the wave number and frequency space. This class of finite difference schemes
69 is generally referred to as dispersion-relation-preserving (DRP) schemes. The radiation
70 and outflow boundary conditions are derived from the asymptotic solutions of the Euler
71 equations, as described by Tam *et al.* [1998].

72 Following a perturbative approach similar to that of Morris *et al.* [1997], the partial
73 differential equations are given by a conservative form of two-dimensional nonlinear Euler
74 equations in which the velocity, pressure and density are given by the sum of the mean
75 flow (the atmosphere) and the disturbance. **These equations are expressed in a**
76 **cartesian coordinate system. The spatial variability of atmosphere and non-**
77 **linear effects are respectively modeled by spatial derivatives and products of**
78 **primitive variables.** Moreover, by using a DRP finite difference scheme, one is assured

79 that the numerical solutions will have the same number of wave modes and the same wave
80 speeds as those of the solutions of the Euler equations, namely, the acoustic, entropy, and
81 the vorticity waves .

82 **Previous work by others in the acoustics community have included non-**
83 **linear phenomena as those of Sparrow and Raspet [1987], but their simula-**
84 **tions contained only up to second order nonlinear terms. In other works,**
85 **modified Burgers equations have been developed and solved for quite specific**
86 **cases. More detailed explanations of these models can be found in the work by**
87 **Cleveland [1996]. However these methods model only one-dimensional acous-**
88 **tic propagation and cannot predict neither the emergence of turbulences due**
89 **to fine layered atmospheric data, nor the (nonlinear) interaction of infrasounds**
90 **with turbulence.**

4. The Misty Picture experiment

91 The Misty Picture experiment was a high explosive test that provided the scaled equiv-
92 alent airblast of an 8 kt nuclear device, on May 14, 1987 (see Reed *et al.* [1987]). Although
93 there was some ambient noise, good microbarograph records were obtained by the French
94 Atomic Energy Commission CEA, the Sandia and Los alamos National Laboratories.
95 **First simulations based on asymptotic techniques were realized by Gainville**
96 ***et al.* [2006].**

97 In the Misty Picture experiment, the structure of the lower atmosphere is known from
98 radio and rocket soundings. The figure 1 shows the wind and temperature profiles used
99 in our computations. Note that the statistical data used to model the upper atmosphere

100 provide winds that are not coherent with both the radiosonde measurements and the
101 meteorological reanalysis. The statistical data are empirical reference models, known
102 as HWM-93 (Horizontal Wind Model) and MSIS-90 (Mass Spectrometer and Incoherent
103 Radar Model). These models represent a smoothed compromise between the original
104 data sources, and are known to present some systematic differences, particularly near
105 the mesopause, as noted by Hedin *et al.* [1996]. Similar arguments have recently moti-
106 vated the atmospheric specification system (G2S) of Drob & Picone [2003] **and the use**
107 **of infrasound technology to probe high-altitude winds (see Le Pichon *et al.***
108 **[2005])**. In our study, the statistical profiles are matched to cubic spline interpolations
109 of radiosonde and rocketsonde measurements in order to capture small scale features of
110 winds. For altitudes higher than 180 km, profiles are continued through a region where
111 a **variable artificial damping similar as that described by Tam & Shen [1993]**
112 **eliminates spurious spatial oscillations of computations.**

113 The acoustic source that models the explosion is obtained from the signal that was
114 recorded at Adminpark which was a station of the Sandia National Laboratory located at
115 about 7 km away from ground zero (see Reed *et al.* [1987]). Following the spectrogram en-
116 ergy distribution of the recorded signal, the waveform used in our computations at ground
117 zero is obtained from the 0.4 Hz filtered Kinney model (see Kinney and Graham [1985]),
118 by modifying the amplitude to obtain back the Adminpark amplitude measurement.

5. Discussion

119 The main effect of atmosphere is the refraction due to sound and wind field gradients
120 and can be computed by using a ray tracing, as shown by red circles in figure 2 that give

121 arrivals. The location and evolution of wavefronts follow some atmospheric structures
122 which may have spatial scales significantly larger than the conventional wavelengths. The
123 results obtained with the DRP finite difference scheme are given by blue lines in figure 2(e).
124 We find multiple arrivals corresponding to a stratospheric phase (Is) and a thermospheric
125 phase (It). The “V” shape of the arrival associated with the thermospheric phase comes
126 from a cusp singularity that we can identify in figure 2(c). An overall good agreement
127 with the ray tracing is obtained except in some large regions of space-time diagram, where
128 the ray tracing fails to predict even the first order disturbance.

129 According to signals obtained with the DRP finite difference scheme, it **appears** that
130 most arrivals of the ray tracing should be continued into the space-time diagram in order to
131 explain the measurements. For example, the first stratospheric phase arrival extends from
132 about 100 km to 500 km which is at least five times larger than the ray tracing predictions.
133 This is clearly manifested in figure 2(e), where the signal recorded at the Roosevelt station,
134 located at 416 km away from ground zero, is compared to our numerical results. **Note**
135 **also that some branches cannot be predicted by the ray method. The reason is**
136 **that, when the acoustic wavefront reaches the upper stratospheric waveguide,**
137 **a small amount of energy radiates in the lower thermospheric waveguide, by**
138 **a diffraction-like phenomenon. This physical mechanism may be described**
139 **by a stratospheric-thermospheric transition $Is \mapsto Is+It$, that involves new**
140 **branches in the space-time diagram. It is typically the case of arrivals located**
141 **at distances between 400 and 700 km, at about 500 sec.**

142 Although the shadow region is a well-defined structure in high frequency approxima-
143 tion, it is not clear how its boundaries vary in presence of small-scale atmospheric inho-
144 mogeneities and more generally the way such regions disappear at low frequencies is a
145 critical problem for infrasonic propagation. In the present study, the three-dimensional
146 shadow region is obtained by using a normal mode technique. The numerical procedure
147 is based on a spectral collocation discretization through a multiple domain technique (see
148 Khorrami *et al.* [1989] and Malik [1990]). The essential contrast with ray tracing is that
149 transmission loss distributions can be computed at distances less than about 250 km,
150 especially in the frequency band 0.1-1 Hz, as shown in figure 3(c). The transmission loss
151 is defined by $TL = 20 \log_{10}(p/p_0)$, where p is the root-mean-square intensity of pressure
152 fluctuations at a field point, with $p = p_0$ (i.e. $TL = 0$ dB) at 1 m from source.

153 The transmission loss distributions together with signals obtained with the DRP finite
154 difference scheme prove that the ray tracing cannot predict the waveforms of microbaro-
155 graph measurements of stations located at River Side (150 km), Silver City (175 km) and
156 Los Alamos (251 km). For frequencies less than 1 Hz or so, the normal mode calculations
157 exhibit some energy at the Los Alamos station, a result which is confirmed by the micro-
158 barograph measurement. For lower frequencies, **a significant amount of** energy may
159 also reach the River Side station, as shown in figure 3(c). This new arrival **exhibits a**
160 **local breakdown of the ray-approximation at frequencies less than 0.4 Hz.**

161 Numerical computations of the pressure field have been carried out up to 1 hour after
162 the wavefront generated by the detonation leaves the computational domain. Figure 4
163 shows a typical set of results about 20 minutes after the wavefront reaches the Barstow

164 station, located at 962 km from ground zero. **We see** from this figure that large-scale
165 coherent structures of atmospheric turbulence develop up to 100 km altitude, mainly in
166 the stratospheric jet, at 70 km altitude, and within small structures of the zonal flow
167 profile, between the tropopause and the matching altitude with smooth statistical data.
168 For unbounded stratified shear flows, it is known that these disturbances are either spon-
169 taneously generated at shear layers or forced outside of them (see Huerre & Rossi [1998]
170 for a detailed review). Due to the presence of shear layers, the stratospheric jet acts
171 as a noise amplifier, that is, infrasounds generated by the detonation may be seen as a
172 controlled forcing for the instability waves.

6. Conclusion

173 In this paper, the long-range propagation of infrasound through a realistic atmosphere
174 is investigated. It is found that for the range of frequency 0.1-0.4 Hz, high frequency
175 approximations of the wave equation do not predict the correct space-time dynamics of
176 infrasounds. **Significant improvements have been obtained by computing the**
177 **solution of non linear Euler equations with a Dispersion-Relation-Preserving**
178 **(DRP) numerical scheme. In particular, new arrivals and large-scale struc-**
179 **tures of turbulence have been computed. According to the instability wave**
180 **theory, these large-scale turbulent structures are directly due to the presence**
181 **of fine scale structures of horizontal components of winds and only disappear**
182 **when using statistical fields. Therefore, depending on the resolution of meso-**
183 **spheric data, hydrodynamic waves may develop higher in the atmosphere and**
184 **interact with incoming low frequency acoustic waves.**

185 With the advent of large parallel computing systems and high resolution meteorological
186 data, the DRP solver constitutes a realistic alternative approach for the three-dimensional
187 propagation of infrasounds through realistic atmospheres, including the background noise
188 of turbulences.

189 **Acknowledgments.** The author is grateful to Dr. E. Blanc for giving him microbaro-
190 graph measurements of the Misty Picture experiment. The authors warmly acknowledge
191 Dr. X. Gloerfelt for providing the DRP algorithm.

References

- 192 Attenborough K., Taherzadeh S., Bass H. E., Raspet R., Becker G. R., Gúdesen A.,
193 Chrestman A., Daigle G. A., L'Espérance A., Gabillet Y., Gilbert K. E., Li Y. L.,
194 White M. J., Naz P., Noble J. M., Van Hoof H. A. J. M. (1995) Benchmark cases for
195 outdoor sound propagation models, *J. Acoust. Soc. Am.* 97(1), 173–191.
- 196 Bogey C. and Bailly C. (2004), A family of low dispersive and low dissipative explicit
197 schemes for flow and noise computations, *J. Comput. Phys.* 194, 194–214.
- 198 Cleveland R. O. (1996), Time domain modeling of finite-amplitude sound in relaxing
199 fluids, *J. Acoust. Soc. Am.* 99, 3312–3318.
- 200 Drob D. P., Picone J. M. and Garcès M. (2003), Global morphology of infrasound propa-
201 gation, *Journal of Geophysical Research* 108(D21), 1–12.
- 202 Gainville O., Piserchia P. F., Blanc-Benon P. and Scott J. (2006), Infrasound propagation
203 in realistic atmosphere: numerical modeling using ray theory and comparison with
204 experiments, *12th Long Range Sound Propagation Symposium*, 1–19.

205 Hedin A.E., Fleming E.L., Manson A.H., Schmidlin F.J., Avery S.K., Clark R.R., Franke
206 S.J., Fraser G.J., Tsuda T., Vial F. and Vincent R.A, (1996) *J. Atmos. Terr. Phys.* 58,
207 1421–1445.

208 Huerre P. and Rossi M. (1998), Hydrodynamic instabilities in open flows. In *Hydrodynam-*
209 *ics and Nonlinear Instabilities* (ed. C. Godrèche & P. Manneville), 81–294. Cambridge
210 University Press.

211 Khorrami M. R., Malik M. R. and Ash R. L. (1998), Application of spectral collocation
212 techniques to the stability of swirling flows. *J. Comput. Phys.*, 81,206–229.

213 Kinney K. J. and Graham G. F. (1985), Explosive Shocks in air. *Springer-Verlag*.

214 Kulichkov S. N. (1992), *Izvestiya, Atmospheric and Oceanic Physics*, 28,253–?.

215 Kulichkov S. N., Avilov K. V., Bush G. A., Popov O. E., Raspopov O. M., Baryshnikov A.
216 K., Re Velle D. O. and Whitaker R. W. (2004), On anomalously fast infrasonic arrivals
217 at long distances from surface explosions, *Izvestiya, Atmospheric and Oceanic Physics*,
218 40(1), 1–9.

219 Kulichkov S. N., Avilov K. V., Popov O. E., Otrezov A. I., Bush G. A. and Baryshnikov
220 A. K. (2004), Some results of simulation of long-range infrasonic propagation in the
221 atmosphere, *Izvestiya, Atmospheric and Oceanic Physics*, 40(2), 202–215.

222 Kulichkov S. N., Bush G. A. and Svertilov A. I. (2002), New type of infrasonic arrivals
223 in the geometric shadow region at long distances from explosions (2002), *Izvestiya*,
224 *Atmospheric and Oceanic Physics*, 38(4), 397–402.

225 Le Pichon A., Blanc E., Drob D., Lambotte S., Dessa J. X., Lardy M., Bani P. and
226 Vergnolle S. (2005), Infrasonic monitoring of volcanoes to probe high-altitude winds,

227 *J. Geophys. Res.*, 110, D13106, doi:10.1029/2004JD005587.

228 Malik M. R. (1990), Numerical methods for hypersonic boundary layer stability, *J. Com-*
229 *put. Phys.*, 86, 376–413.

230 Morris P., Long L., Bangalore A. and Wang Q. (1997), A parallel three-dimensional
231 computational aeroacoustics method using nonlinear disturbance equations, *J. Comp.*
232 *Phys.*, 133, 56–74.

233 Ponomarev E. A., Rudenko G. V., Sorokin A. G., Dmitrienko I. S., Lobycheva I.Y. and
234 Baryshnikov A. K. (2006), Using the normal-mode method of probing the infrasonic
235 propagation for purposes of the comprehensive nuclear-test-ban-treaty, 68, 599–614.

236 Raspet R., Baird G. E. and Wu W. (1992), Normal mode solution for low-frequency sound
237 propagation in a downward refracting atmosphere above a complex impedance plane,
238 *J. Acoust. Soc. Am.* 91(3), 1341–1352.

239 Raspet R., Baird G. E. and Wu W. (1991), The relationship between upward refraction
240 above a complex impedance plane and the spherical wave evaluation for a homogeneous
241 atmosphere, *J. Acoust. Soc. Am.* 89(1), 107–114.

242 Reed J. W., Church H. W. and Huck T. W. (1987), Misty Picture weather-watch and
243 microbarograph projet, *SAND87-2978C*.

244 Sparrow V. W. and Raspet R.(1991), A numerical method for general finite amplitude
245 propagation in two dimensions and its application to spark pulses, *J. Acoust. Soc. Am.*
246 90, 2683–2691.

247 Tam C. K. W. and Webb J. C. (1993), Dispersion-Relation-Perserving finite difference
248 schemes for computational acoustics, *J. Comput. Phys.* 107, 262–281.

249 Tam C. K. W., Webb J. C. and Dong Z. (1993), A study of the short wave components
250 in computational acoustics, *J. Comput. Acoustics* 1, 1–30.

251 Tam C. K. W. and Shen H. (1993), Direct Computation of nonlinear acoustic pulses using
252 high-order finite difference schemes. *AIAA Paper 93-4325*.

253 Tam C. K. W. and Dong Z. (1996), Radiation and outflow boundary conditions for direct
254 computation of acoustic and flow disturbances in a nonuniform mean flow, *J. Comput.*
255 *Acoustics* 4(2), 175–201.

256 Tam C. K. W., Fang J. and Kurbatskii K. A. (1998), Non-homogeneous radiation and
257 outflow boundary conditions simulating incoming acoustic and vorticity waves for ex-
258 terior computational aeroacoustics problems, *Int. J. for Num. Methods in Fluids* 26,
259 1107–1123.

260 Whitham G. B. (1974), Linear and non linear waves, *Wiley-Interscience, New-York*.

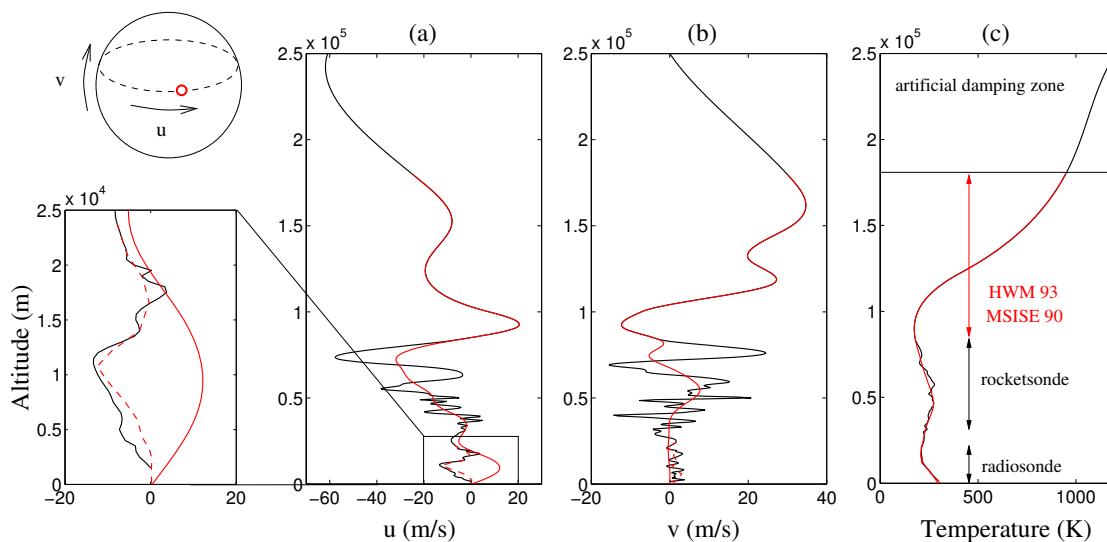


Figure 1. Wind and temperature profiles at ground zero used for the Misty Picture computations. (a) : East (zonal) wind component ; (b) : North (meridian) wind component. The solid black line and the solid red line give respectively the profiles used in the computations and the statistical profiles (HWM-93, MSIS-90). The dashed red line corresponds to a meteorological reanalysis.

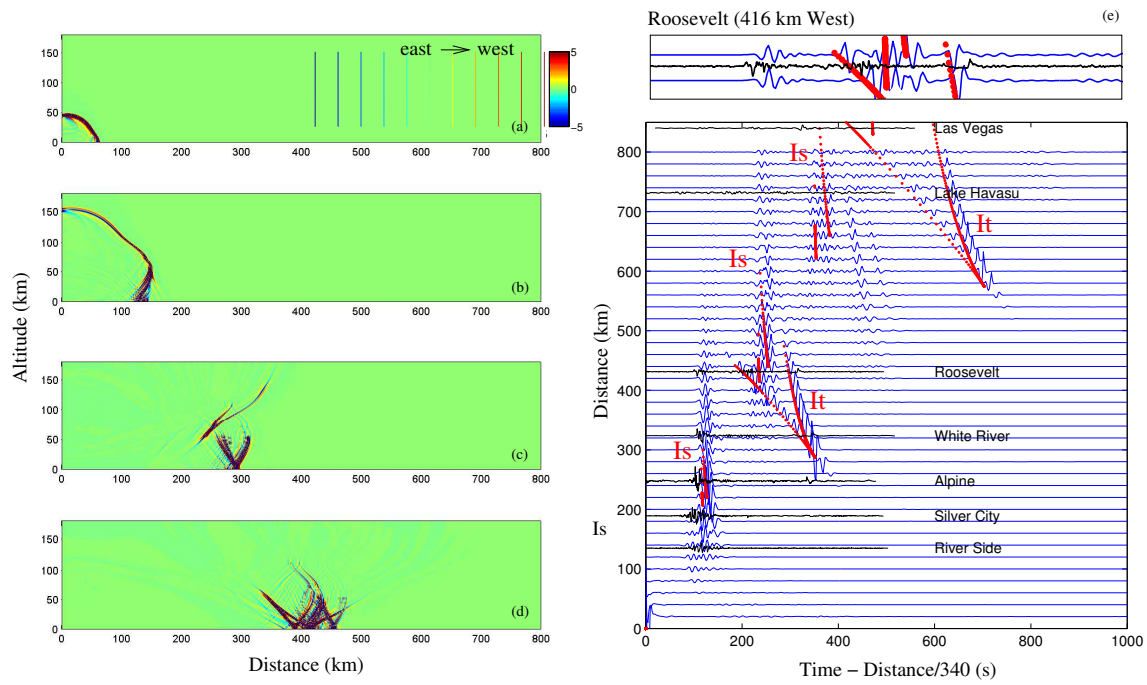


Figure 2. Wavefronts (colors range from -5 to 5 Pa) at different times (a-d) and ground waveforms (e) obtained with the DRP scheme. **The flow is given by the zonal component u .** The measured signals and the arrivals given by the ray tracing are respectively shown by the solid black lines and the red circles.

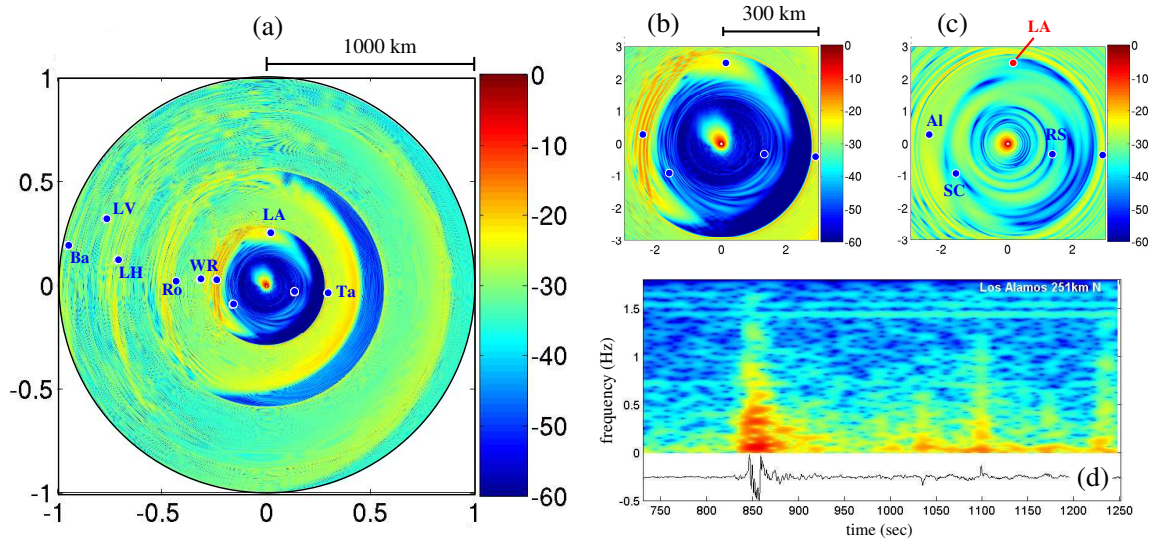


Figure 3. Transmission loss obtained by a normal mode technique for 1.0 Hz (a,b) and 0.1 Hz (c). The blue circles give the location of stations River Side (RS), Silver City (SC), Alpine (Al), Los Alamos (LA), White River (WR), Roosevelt (Ro), Lake Havasu (LH) and Las Vegas (LV). The spectrogram obtained from measurement at Los Alamos is given in (d).

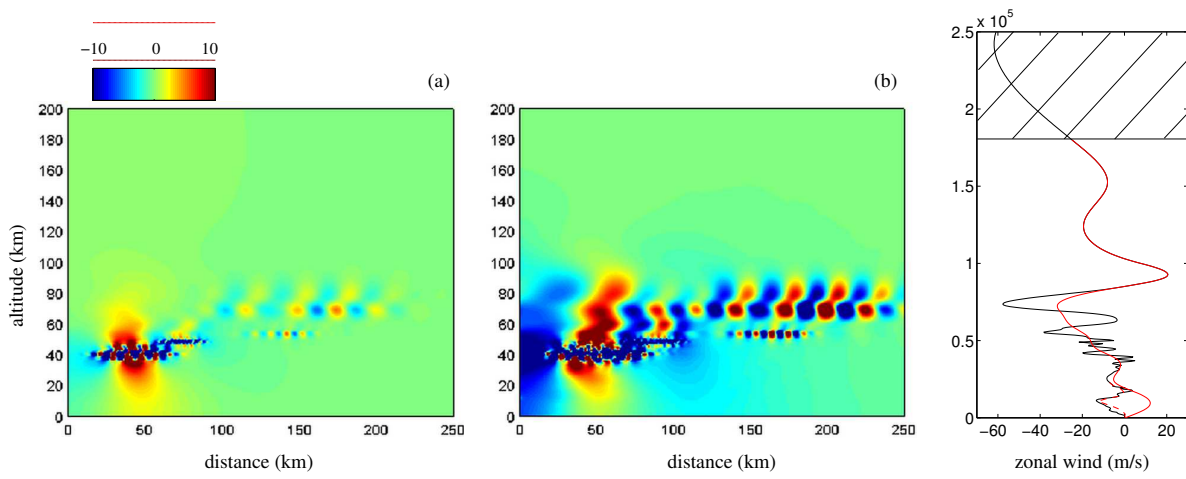


Figure 4. Large-scale structures of stratospheric turbulence developing in small-scale atmospheric mixing layers. Simulation snapshots are given for $t = t_0 + 4800$ s (a) and $t = t_0 + 5600$ s (b), where t_0 is the Misty Picture explosion time. Colors range from -10 Pa to 10 Pa.